



The most extreme heat waves in Amazonia happened under extreme dryness

Duarte F. Costa^{1,2} · Helber B. Gomes² · Maria Cristina L. Silva² · Liming Zhou³

Received: 14 November 2020 / Accepted: 29 December 2021

© The Author(s), under exclusive licence to Springer-Verlag GmbH Germany, part of Springer Nature 2022

Abstract

Heat waves in Amazonia have become more frequent, longer, and more intense according to observational records. Climate change and deforestation are two significant drivers of such trends. In the Amazon rainforest, heat waves are still an understudied issue, in part due to limited surface observations. To date, heat waves in central Amazon have been associated with the ITCZ northward migration in austral winter, weakening moisture influx through the South American Monsoon System. This study contributes to this topic by being the first Amazon-specific analysis of heat extremes and the first in South America to jointly explore extreme heat wave events and associated synoptic atmospheric and land surface conditions. Ten of the most extreme heat waves are identified in the Southeast of Amazonia, from Era-Interim (1979 to 2018) maximum daily temperature records. Dry conditions are measured from relative humidity and evaporative fraction anomalies at surface and vertically also using the Era-Interim data. In all 10 events an extreme drying signal co-occurs with extreme heat waves. Wind patterns and anomalies revealed a consistent easterly dry advection anomalously extending to Southeast Amazonia. In addition, an intensification of the northerly South Atlantic Anticyclone wind circulation reduced the influx of moisture to Southeast Amazon, namely linked to the South American Low Level Jet. These, together, contributed to a compound effect on the extreme heat waves under near-surface drying conditions, which escalated hot temperatures to extreme heat.

Keywords Amazon rainforest · Heat wave · Drought · Extreme weather · Land-surface · South America

1 Introduction

Recent studies using different types of observational datasets have been pointing towards a warming trend in South America (Almeida et al. 2017a, b; Marengo et al. 2018; de Barros Soares et al. 2017), that is unparalleled elsewhere in the global tropics (IPCC 2013, Technical Summary, Fig TS 2). Within South America, such a warming trend goes up to 1 °C/decade over the period 1975–2004 (de Barros Soares et al. 2017), particularly over the southern and eastern frontier of the Amazon, also known as the Arc of Deforestation.

This warming rate is exponentially faster than the global average of 0.15–0.2 K/decade (Observatory 2010). Warming trends are particularly evident during the dry season (JJA and SON) in this region extending into both the Amazon and the Cerrado sides of the Arc. Part of this region is made of floodplain forests which are highly sensitive to drought and warming, having recently been coined as the *Achilles heel of Amazonian forest resilience* (Flores et al. 2017). Negative trends in dry season rainfall (Alves et al. 2017; Espinoza et al. 2018; Gloor et al. 2015), extreme droughts, and warming trends have been found to happen in tandem in observational and reanalysis data. For example, the largest warming trends occur during the dry season, especially in the southeast of Amazonia, and the hottest years are years of extreme drought (Jiménez-Muñoz et al. 2013). More recently, after one of the strongest El Niño events on record in 2015/16, it was found that record breaking warming during the dry season co-occurred under conditions of extreme drought in the strongest recent El Niño years (Jiménez-Muñoz et al. 2016).

Trends in extreme temperatures are harder to estimate because long uninterrupted observations are required

✉ Helber B. Gomes
helber.gomes@icat.ufal.br

¹ Stantec Belgium, Av. Reine Astrid 92, 1310 La Hulpe, Belgium

² Institute of Atmospheric Sciences, Federal University of Alagoas, Alagoas, Brazil

³ Department of Atmospheric and Environmental Sciences, University at Albany, State University of New York, New York, NY, USA

but these events occur seldomly. Observational datasets for Amazonia are very limited (Hartmann et al. 2013), Table 2.13, IPCC 2013, Technical Summary, Fig TS 2). Nevertheless, it is still possible to use the available station data to confirm this tendency and point towards a significant warming of heat extreme features in the tropical north of the domain, namely over the Amazon and the Northeast of Brazil (NEB) (Skansi et al. 2013).

Global climate models also confirm this trend in South America: using an ensemble of CMIP5 coupled climate models, (Donat et al. 2017) identify a significant signal in South America as one of the regional hotspots of accelerated warming where heat extremes have been increasing at a faster pace than mean temperature. This is specifically the case for the Arc of Deforestation region particularly in Southeast Amazon and in the Cerrado. Unfortunately, due to the lack of consistent observations, the researchers were not able to determine if this signal in models was inconsistent with observations as it was for some of the other hotspots identified elsewhere. These model simulations also showed that, heat extremes were aggravated due to extreme drying surface, leading to a heat amplification from reduced evaporative fraction, particularly over Eastern and Central Amazonia and the Cerrado.

The Eastern frontier of Amazonia is characterized as one of the driest climates within the Amazon floodplain (Salati et al. 1979), with some of the lowest observed annual rainfall totals around 1600 (Leopoldo et al. 1987) to 1800 (Borma et al. 2009) mm/year. The dry season is also amongst the longest within the Amazon basin floodplain which can last for up to 6 months with rain below 100 mm/month (Restrepo-Coupe et al. 2013). Such a prolonged dry season with little or no rain and highly permeable sandy soil leads to a rapid depletion of soil moisture and, unlike in the rest of Amazonia, to lower evapotranspiration (ET) in the dry season than in the wet season (Da Rocha et al. 2009; Borma et al. 2009). Such reduction in ET, triggers at the surface energy balance and causes an increase in sensible heat and decreases Evaporative Fraction (EF) as a result of lower latent heating from ET. This is the key land-surface biophysical feedback from a dry land surface amplifying surface heat which, depending on the synoptic settings, can be conducive to an escalation of hot temperatures to extreme heat (Miralles et al. 2014; Perkins 2015; Fischer et al. 2007; Hirsch et al. 2015; Duan et al. 2020; Bryne 2021). Most extreme weather events are often driven by anomalous large-scale atmospheric circulation. The synoptic patterns of the dry season are associated with the South American Monsoon System (SAMS) which is highly linked to the northward migration of the ITCZ during JJA (Espinoza et al. 2011). A weaker SAMS during the dry season reduces the influx of moisture into the Amazon, creating conditions for dry weather where intense solar radiation rises daily maximum

temperatures. Some of the synoptic mechanisms of heat-waves are shared with those of drought, such as the northward seasonal shift in the ITCZ position. In the limited literature available analysing heat extremes in the Amazon, this has been pointed as the key synoptic driver of heatwaves in this region (Bitencourt et al. 2016; Geirinhas et al. 2018), yet this seasonal pattern does not explain alone the occurrence of extreme heat at the end of the dry season. Elsewhere in the mid-latitudes, heat waves are linked to dry surface conditions. Yet, this association has never been identified in the context of Amazon. Indeed, the occurrence of the hottest days and events of the year in the Amazon is more complex than that. The ITCZ northward maximum occurs around late June and early July, around the June solstice. Yet the hottest month of the year in Amazonia varies from late August in central to western Amazonia to mid September in the southeast. In fact, during these months, the ITCZ is again on a southbound trajectory to its southern maximum around the December solstice.

Hence, while the ITCZ northward migration and variability are an important mechanism to explain the drying and weakening of the SAMS, it does not fully explain the occurrence of heat waves and their synoptic footprint.

The weakening of the SAMS has a visible effect in the seasonal cycle of the moisture load of the South Atlantic Convergence Zone (SACZ) and the circulation pattern of the South American Low Level Jet (SALLJ) (Montini et al. 2019; Marengo et al. 2004). The SALLJ is one of the most important elements of South American mesoscale circulation, especially as a key conveyor of moisture from Amazonia to the south of South America (Silva, et al. 2009; Marengo et al. 2004). The SALLJ is a southern branch of the ITCZ and one of the key low level circulation streams of the SAMS that, during most of the year (especially during the wet season in DJF), travels southwestwards from the Amazon basin into the Andes foothills. The Andes deflect the SALLJ southeastwards into the southern parts of South America (such as the Southeast of Brazil (SeB) and the La Plata basin (LPB)) enabling a crucial drainage of moisture into these regions (Marengo et al. 2004; Liebmann and Mechoso 2011).

During the dry JJA and SON seasons the weakening of SAMS and strengthening of the South Atlantic Anticyclone (SAA) decreases convective instability and shifts southwards (away from the southeast of Amazonia) the SALLJ northeastern transport of air and moisture. Furthermore, this anticyclonic intensification of the SAA usually at a position nearer to the Brazilian coast makes the western branch of this anticyclone to advect easterly into the NEB and occasionally into the Amazon (Gomes et al. 2019), feeding dry air into the SALLJ circulation. Indeed, during JJA, the percentage of SALLJ days is the highest in the year with about 15–20% of days being SALLJ days (Montini et al. 2019).

Yet, this jet is much drier than during the SAMS' strongest seasons (DJF and MAM) and shifted southwards.

The end of the dry season (JJA) and beginning of shoulder season (SON) is the annual moment when these dry season synoptic mechanisms coincide with extreme dryness at surface as a result of a prolonged dry season. This is the reason why the hottest season of the year in Southeast Amazon occurs in August and September. Heat extremes in the Amazon are inevitably closely related to the length and intensity of the preceding dry season which is per se dependent on surface (soil and vegetation) moisture levels recharged during the preceding wet season (Marengo et al. 2011, 2018; Da Rocha et al. 2009; Borma et al. 2009). Antecedent conditions, from inter-seasonal to inter-annual timescales, have been observed to play a critical role for the amplification of surface temperature to extreme heat in different transition environments (Ukkola et al. 2018). However, in the context of the Amazon, this has not been so far illustrated.

In this paper, extreme heat and dryness are jointly analysed in a sub-section in the southeast of Amazonia, where the largest warming trends were found (Jiménez-Muñoz et al. 2013). The next section introduces and explains the Data and Methodology used. The Results and Discussion are presented together introducing the maximum, minimum temperature and surface dryness features of one of the 10 heatwaves identified (the remaining are illustrated in the supplementary material) as well as the mean patterns and anomalies of wind circulation and vertical profiles of relative humidity. The paper concludes with bringing together the different components of evidence from surface dryness to atmospheric circulation in explaining the occurrence of heat waves, raising as well the limitations and future pathways to continue research in this new field in Amazonia.

2 Data and methodology

2.1 Southeast Amazon

A subsection in the southeastern frontier of the Amazon was selected where the strongest signal of longer and more intense heat wave anomalies within the Amazon basin was found. This subsection will be called here Southeast Amazon covering 8° to 12° S and 60° to 50° W. It comprises 70 grid cells at 0.79° × 0.79° in the southeastern most end of the Amazon where vegetation in Era-Interim data (described below) is above 97% of evergreen broadleaf trees (rainforest) cover.

2.2 Era-Interim data

The ERA-Interim data (hereafter called ERAI) is a reanalysis product produced by the European Centre for

Medium-Range Weather Forecasts (ECMWF) using a numerical weather prediction (NWP) model to simulate the historical climate *constrained* by observational data *assimilated* into the Integrated Forecasting System (IFS) model simulation (Dee et al. 2011). In order to optimize the *assimilation* of observations with the NWP model IFS simulation, ERAI uses a complex four-dimensional variational analysis (4D-Var) system to find an optimal fit through all the observations in the assimilation time window (Bannister 2001). The 4D-Var analysis takes the IFS dynamics and physics to generate a sequence of states optimally fitting the atmospheric observations.

The robustness of ERAI assimilation has been found to be one of the most accurate reanalysis of surface temperature and temperature variability, both globally (Decker et al. 2012) and in South America (de Almeida et al. 2017a, b; Lorenz & Kunstmann 2012). Daily mean values from ERAI reanalysis were extracted from the period from 1979 to October 2018 at a spatial resolution of 0.79° × 0.79° (Dee et al. 2011). Anomalies were calculated with reference to the 30-year climatological calendar-day baseline of 1979–2009 for the South American region using the CORDEX-South America domain as a coordinate reference (90° W, 30° W; 20° N, 60° S).

Land–Atmosphere parameters.

The following land–atmosphere variables were used to evaluate the heat extremes from the ERAI data:

- Daily Maximum Temperature (Tasmax)
- Daily Minimum Temperature (Tasmin)
- Relative Humidity (hur)
- Solar radiation at surface (downwards at 12h00 Brasilia Time (BRT))
- Evaporative Fraction (EF)
- Wind vector fields

2.3 Heat wave definition

Heat extremes are identified as an extended period of hot weather relative to the expected conditions of a given site and season. Different definitions exist focusing on different implications that heat waves can have, particularly adopting different thresholds from which weather is classified as extremely hot. Thresholds can be set as absolute markers (for instance when a physical absolute threshold is known to trigger a specific reaction or impact) or a relative threshold (for instance a top percentile of a distribution). The latter allows for comparative analysis between sites and to adjust for human acclimatization to extreme weather, which is an important element when assessing human health implications of extreme heat. Here we adopted a relative threshold from a common methodological definition that identifies heat wave periods of at least 3 consecutive days when

anomalies of maximum temperature were among the top 10% hottest days (> Tx90p) in the 30-year climatological period (1979–2009). This has been found to be a frequent criterion for the identification of heat waves in heat extremes literature (Perkins 2015). Heat wave events and maxima were identified for each grid cell in South America and also in Southeast Amazon.

To establish the time series of these events, a regional average over Southeast Amazon was calculated. Caution is necessary when analysing regional means of climate extremes as averaging reduces the signal from an extreme event. In some cases, periods of consistent heat wave days were interrupted by an average daily anomaly falling below the tasmax 90th percentile (p90). To ensure the consistency of a longer heatwave event, consecutiveness was made flexible allowing up to 1 day of non-heat wave conditions during an event, for as long as its intensity was above the tasmin p90.

The p90 was calculated from the distribution of anomalies (1979–2018) of these variables. It identifies the anomaly threshold at which tasmax enters the range of 10% highest anomaly values in each specific location. For variables that are physically anti-correlate with tasmax, the 10th percentile was considered instead. This is the case of relative humidity (RH) and Evaporative Fraction (EF). EF was preferred as a metric of the partitioning of surface heat fluxes and thereby of land surface dryness (Ukkola et al. 2018; Donat et al. 2017). EF was calculated from latent (Le) and sensible heat (H) as:

$$EF = Le / (Le + H).$$

EF ranges between 0 to 1, and describes the partitioning of available energy between Le and H, with low values characterizing dry conditions and high values wet conditions. EF was calculated using Le and H at 15h00 UTC (corresponding to the local noon in the Brasilia time zone (BRT) from ERAI. ERAI surface heat fluxes are *forecast*

data accumulated and written every 3 h. The instantaneous values at $W/m^2/s^{-1}$ were estimated as the average in each period of 3 h which is the shortest time resolution in ERAI forecast data.

The most intense and longest events for each of the 70 grid cells in the Southeast Amazon subregion were identified from the ERAI record. These occurred in 7 different years, six of which in the current decade. All events occurred at the transition from the dry to wet season (between August and November). The events during this season in 2011 and 2015 were particularly long but when averaged across all grid cells in subset they were discontinuous (heat wave days were interrupted by non-heatwave conditions) and as such multiple events were considered in these years. The 10th event (HW10) was selected to feature in the main text of this article since it was i) a record breaking heat wave in terms of duration and intensity and ii) is the most recent event.

Spatial mean anomalies were calculated to identify the mean spatial patterns of temperature and relevant land–atmosphere fields during each heat wave such as relative humidity (RH from *hur* in ERAI data) and EF. Absolute and anomaly wind vector fields were analysed at 850 hPa levels together with surface anomalies of RH and horizontal transport of water vapour (*viewvf*—vertical integral of eastward water vapour flux). Finally, a zonal cross section analysis of relative humidity was conducted along the easterly advection circulation at 10°S to analyse the vertical distribution of humidity above both dry and wet surface region.

3 Results

3.1 Extreme heatwave events

The duration of these events ranges from 5 (HW9) up to 31 (HW10) days (Table 1). Four of these events represented a

Table 1 The list of 10 heat wave events identified and their general characteristics. HW10 is the main event featured in the main text

Event	Start date	End date	Duration (days)	Max anomaly date	Max anomaly (°C)	Max Tasmx (°C)
HW1	03/11/1997	12/11/1997	10	1997–11–09	+7.81*	35.9
HW2**	03/09/2010	29/09/2010	27*	2010–09–16	+7.03*	37.8
HW3	09/08/2011	16/08/2011	8	2011–08–11	+4.14	37.2
HW4	29/08/2011	02/09/2011	5	2011–08–30	+4.91	37.3
HW5*	15/09/2011	26/09/2011	12*	2011–09–25	+6.92	37.6
HW6*	03/09/2012	17/09/2012	15*	2012–09–10	+6.93	38.2
HW7	15/09/2015	21/09/2015	7	2015–09–19	+7.76	37.9
HW8*	13/10/2015	24/10/2015	12	2015–10–22	+9.15*	37.8
HW9	08/09/2016	12/09/2016	5	2016–09–09	+4.47	35.6
HW10**	25/08/2017	24/09/2017	31*	2017–09–19	+7.27*	37.4

*Record breaking events in either intensity, duration, or ** both

new duration record break in a fraction of the grid cells of Southeast Amazon. Some of these events are preceded or succeeded with more heat wave days. But following the principle of consecutiveness, they are not considered as part of the events unless their time periods are consecutive (unless with a 1-day maximum of discontinuity). The timeseries in Fig. 1 (and Fig. S1 to S6 in supplementary material) illustrate these occurrences, particularly in the years of 2011 and 2015. These describe the anomaly conditions during the

same and previous months in which each of the 10 events occurred. In addition, anomaly timeseries of relative humidity, solar radiation, and EF for HW10 are presented.

In terms of intensity, the average anomaly for the 10 events is +6.64°C which is more than the double of the average p90 of +3.2°C. The largest anomalies are found in the months of October and November as these are on average less warm than August and September. This is the case of HW1 and HW8, both being new record breaking events,

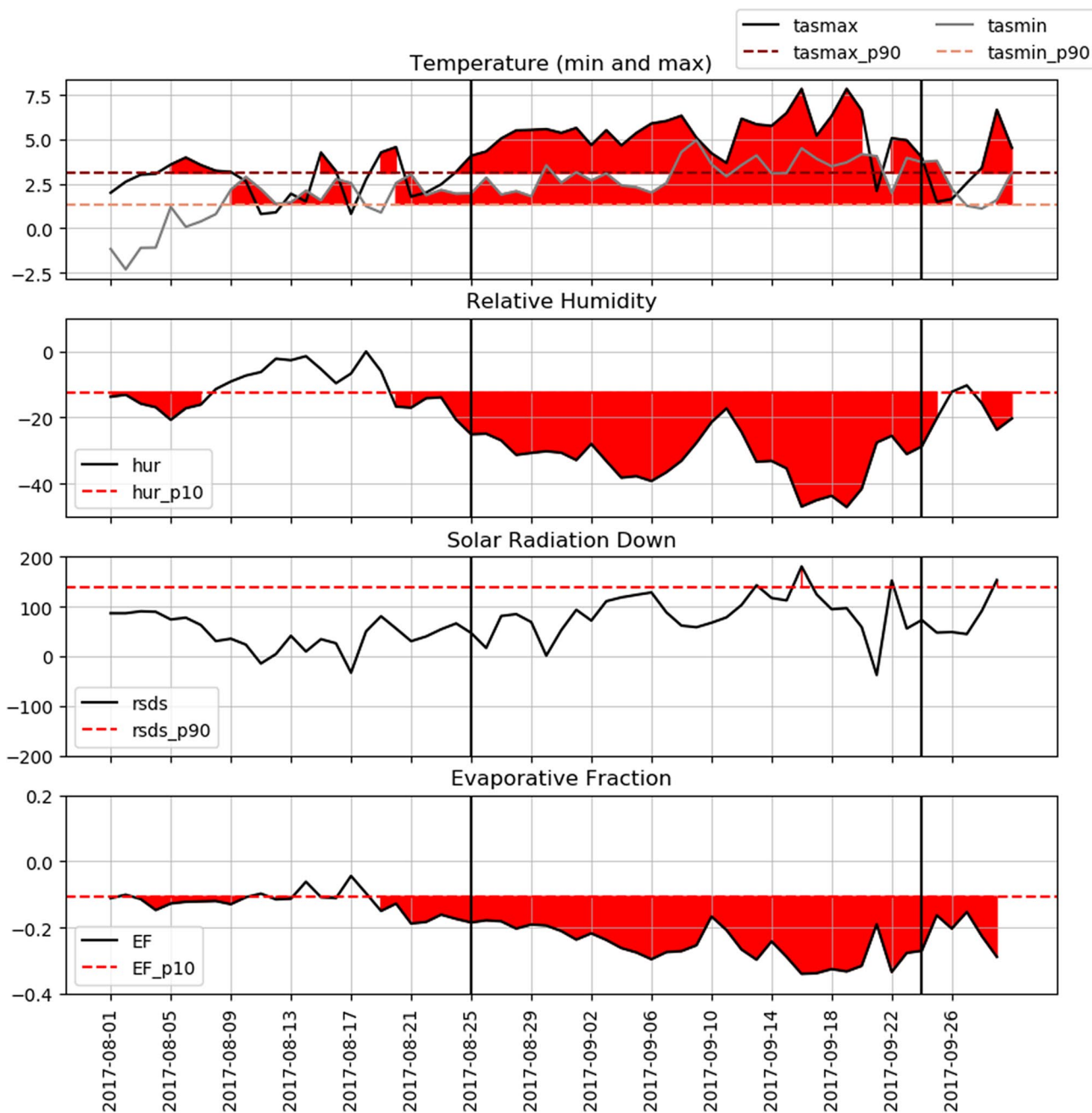


Fig. 1 Timeseries of tasmax and tasmin anomalies during heatwave HW10 along with surface dryness anomalies of RH and EF. Solar radiation anomalies are included as an indication of surface heating anomalies from shortwave radiation

leading to large tasmax temperature anomalies during the shoulder season.

Six of these events were record-breaking events of anomalous intensity and duration in a fraction of gridcells of this subset. Namely HW1, HW2, HW8, HW10 and HW2, HW5, HW6, HW10 respectively. Some of these new records in intensity are visible in Fig. 2 when the regional signal of such an event was large enough to peak the average Southeast Amazon seasonal (ASON) anomalies. Some of the events highlighted in this paper were identified as record breaking events of long or intense heat waves in a fraction of gridcells. Figure 2 is an average of tasmax anomalies for the Southeast Amazon capturing some of the most intensive and extensive heat extremes in this region in the last 40 years. However, not all events resulted in an anomaly peak in Fig. 2 as some were chosen due to their extensive duration or localized (in a few gridcells) record-breaking intensity (e.g. HW6). Similarly, an event in 2007 is captured in this figure that was not identified in the gridcell analysis, due to its short duration and a new record-breaking event surpassing it in 2015.

The most prominent feature among these extreme events is the clear concomitant occurrence of extreme heat and extreme dryness indicated both in EF and RH at surface. This is also spatially clear in the anomaly composite of each event (Figs. 3, 4).

In some of these events, extreme dryness in the land–atmosphere precedes the heat wave for a prolonged period, ranging from 2 to 4 weeks, such as in HW2, HW4, HW5, HW6, and HW10. Furthermore, the highest tasmax anomalies also co-occur with the lowest values of surface and atmospheric relative humidity. In all events tasmin anomalies were above their p90 and in 8 out of 10 events tasmax anomalies surpassed their p90.

Anomalies in 12 UTC downward solar radiation are shown in Fig. 1 (and Figs. S2 to S6): whilst high and near the p90 anomaly threshold, they are within the 10% most extreme anomalies as conversely RH and EF are. This indicates that anomalous extreme heat events may depend more on anomalies in surface dryness than those in solar radiation. To investigate the association among these variables, the correlation coefficient between tasmax anomalies and RH, EF and solar radiation anomalies was calculated during the month of each event and the preceding one (Table 2).

The correlation results show that in all events the anomalies of these three variables are strongly and significantly correlated with the anomalies of tasmax, particularly RH, which has consistently the highest coefficient values. Whilst Table 2 shows the significant relevance of these three variables, particularly of RH, Fig. 1 (and Figs. S1 to S6) highlights the dominant role of extreme dryness in association with the occurrence of extreme heatwaves.

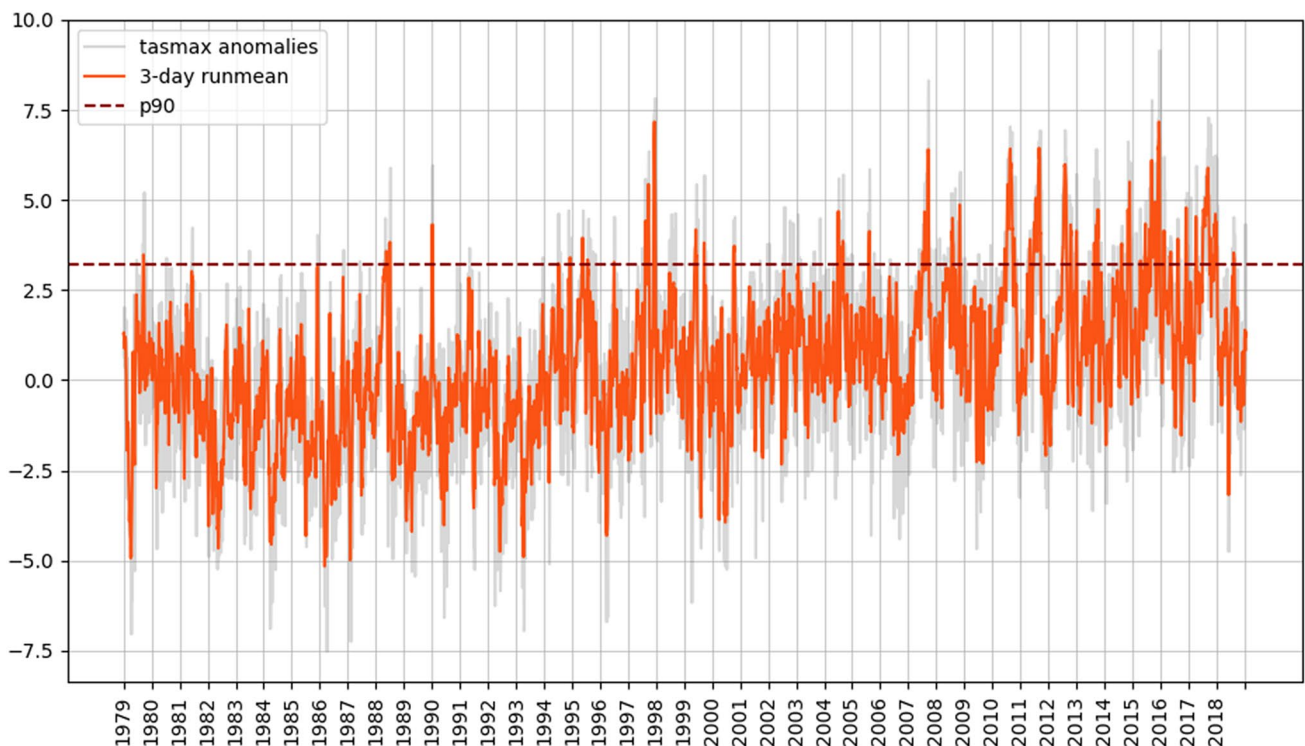


Fig. 2 Tasmax anomalies ($^{\circ}\text{C}$) during the August–November (ASON) heat wave season in Southeast Amazon from 1979 to 2018 (grey). 3-day running mean (orange) and tasmax anomaly 90th percentile (dashed red)

Heatwave anomaly composite maps for 5 heatwaves AMZ

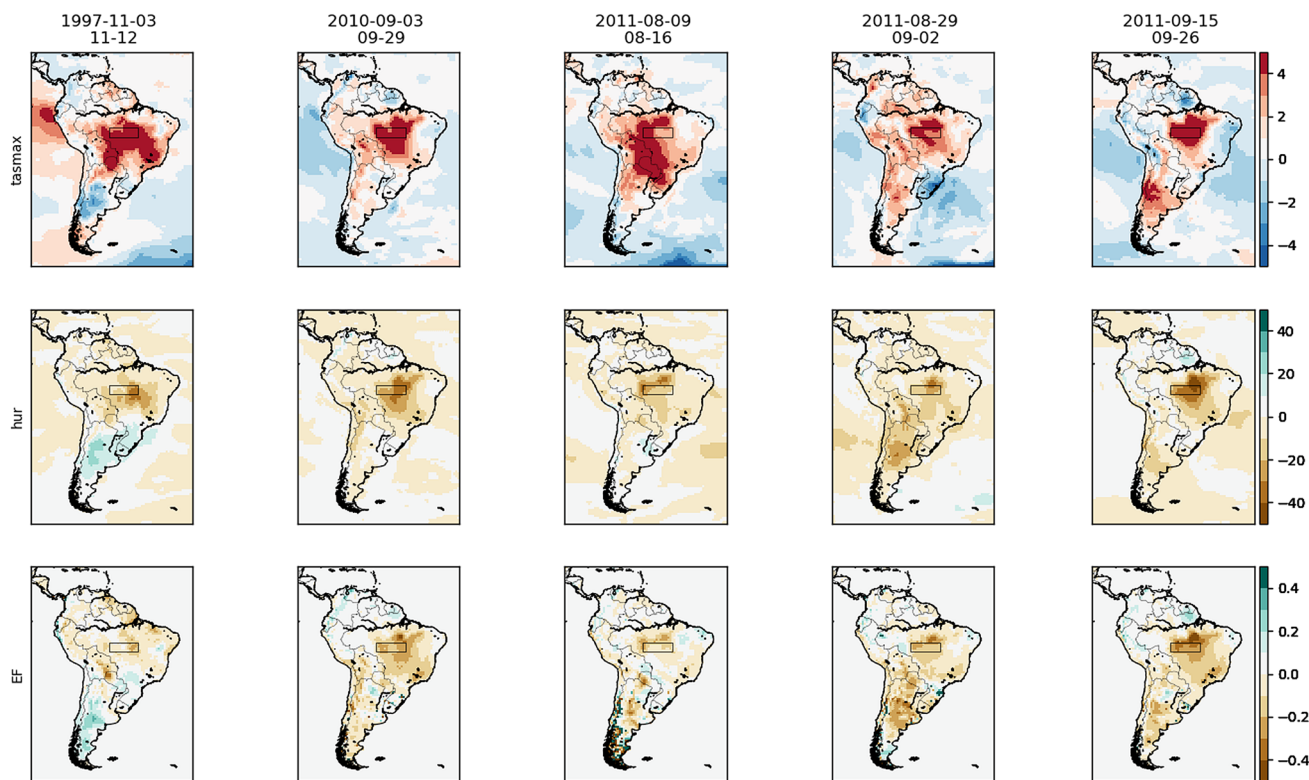


Fig. 3 Average spatial anomalies of near-surface tasmax, RH, and EF during HW1, HW21, HW3, HW4, and HW5

4 Wind patterns and anomalies

The wind patterns and anomalies for HW10 are shown in Fig. 5 and those for the remaining events are shown in Figs. S7 to S24. There are two synoptic patterns emerging from the intensification of the SAA that contribute to increased drying at surface: the easterly advection through the coast of the Northeast of Brazil into the Amazon (Pattern A) and the shift/suppression of the SALLJ flow pattern (Pattern B). These patterns depend on the position and strength of the synoptic conditions that both feed (*push factor*) and pull (*pull factor*) such air motion.

In all 10 events an easterly wind pattern was found, which in 9 out of 10 events is driven by the intensified SAA. A northward wind anomaly was also found in the northern tropical Atlantic along the north coast of South America, indicating a slower return of the ITCZ. In some of these events (HW1, HW2, HW5, HW6, HW7, in Figs. S16, S17, S20, S21, S22, respectively), an eastward anomaly also denotes a weaker ITCZ general circulation.

The main *push factor* for Pattern A is the position and strength of the SAA from which the easterly advection is *pushed* from. The position is consistently found at the same latitude (around 30°S) in all events with slight

differences in its distance to the coast. The mean anomalies show changes in the strength of this anticyclone. In events HW2, HW5 and HW10 an anticlockwise anomaly shows a stronger SAA (Figs. S17, S20, 5b). In HW2 and HW10 it strengthens the easterly advection but also shifts southward the SALLJ flow pattern (B). In HW5 the northbound flow of the SAA slows down the ITCZ return (weakening the SAMS and the *push factor* for B) and shifts SW-wards the *pull factor* for Pattern B.

The SALLJ flow is the key mechanism to transport moisture from the ITCZ and the central parts of the Amazon to the SE of Amazonia and ultimately the Southeast of Brazil (Marengo et al. 2004; Montini et al. 2019). Its main *push factor* during the JJA season is the anomalously slow southbound return of the ITCZ, which in some events is also weakened (weaker trade wind anomalies are found in events HW1, HW2, HW5, HW6, HW7, in Figs. S16, S17, S20, S21, S22, respectively). In 8 out of 10 events, this is associated with the intensification of the SAA wind circulation, which bifurcates in the NEB coast: partly flowing inland westwards into the Amazon (Pattern A), partly flowing directly NW-wards slowing down the southbound return of the ITCZ.

Heatwave anomaly composite maps for 5 heatwaves AMZ

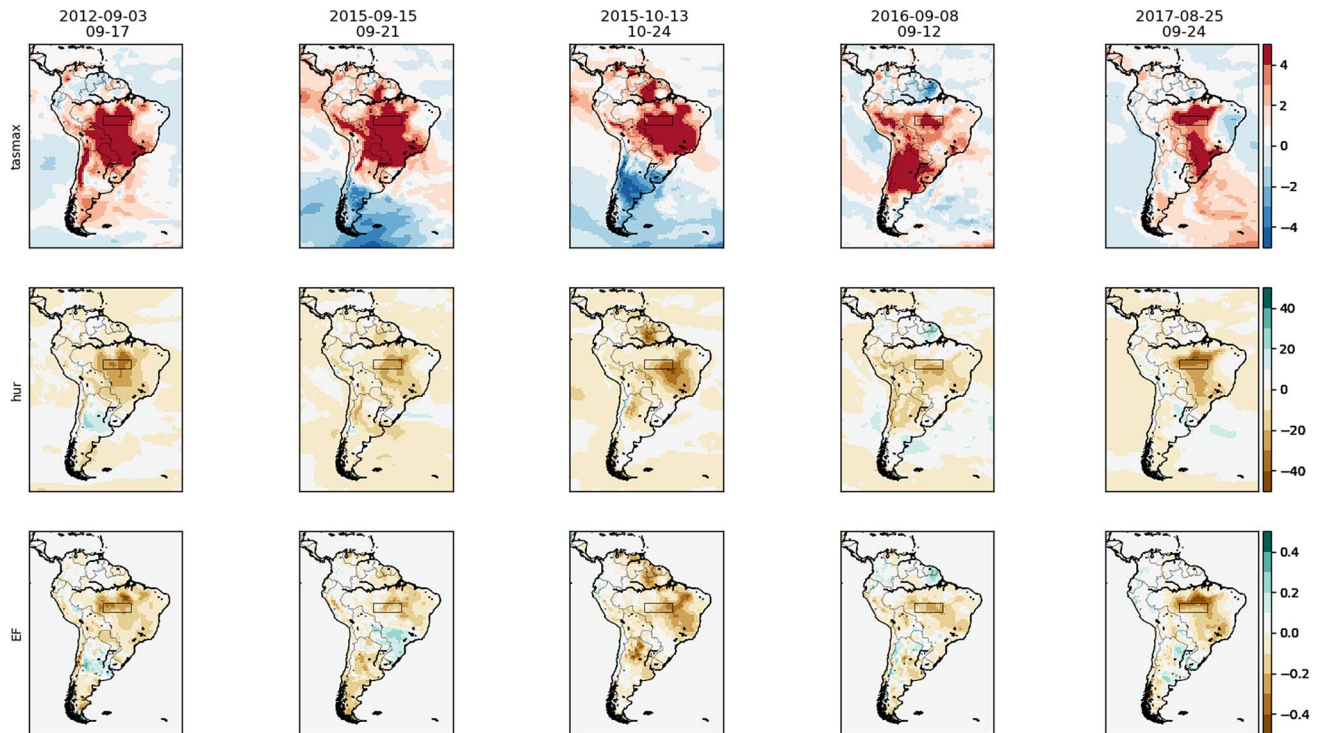


Fig. 4 As in Fig. 3, but for HW6, HW7, HW8, HW9, and HW10

Table 2 Correlation r and p values of RH, EF and solar radiation anomalies with tasmax anomalies during the month of each heat extreme and the preceding one

Event	RH		EF		Solar radiation	
	r	P	R	P	r	P
HW1	-0.94	1.00E-028	-0.81	4.06E-015	0.88	1.93E-020
HW2	-0.71	1.05E-010	-0.69	1.27E-009	0.39	0.0018652
HW3	-0.77	4.91E-013	-0.59	8.69E-007	0.59	5.57E-007
HW4	-0.77	4.91E-013	-0.59	8.69E-007	0.59	5.57E-007
HW5	-0.77	4.91E-013	-0.59	8.69E-007	0.59	5.57E-007
HW6	-0.84	3.27E-017	-0.85	7.14E-018	0.68	1.58E-009
HW7	-0.79	1.05E-027	-0.71	4.66E-020	0.65	5.64E-016
HW8	-0.79	1.05E-027	-0.71	4.66E-020	0.65	5.64E-016
HW9	-0.75	3.32E-012	-0.57	2.03E-006	0.64	4.44E-008
HW10	-0.81	4.62E-015	-0.73	2.87E-011	0.58	1.25E-006

In 8 out of 10 events (HW1, HW2, HW3, HW6, HW7, HW8, HW9, HW10) Pattern B is shifted to a further south position over Paraguay into Uruguay (see positive wind anomalies over this region in Figs. S16, S17, S18, S21, S22, S23, S24 and 5, respectively), steering moisture away from the Southeast of Amazonia. Events HW4 and HW5 are different to this pattern in which the SALLJ flow pattern changes into a different direction (NE \rightarrow SW) – HW5 (Fig S20) – or is suppressed by an alternative synoptic pattern (Low) – HW4 (Fig S19). For the latter, this is

associated with a northward shift of a mid-latitude Low (L) which deflects the Pacific westerly jet on a SW \rightarrow NE trajectory blocking any flow for Pattern B from both normal (NW \rightarrow SE) or shifted (N \rightarrow S) SALLJ conditions. Hence, despite different synoptic structures the effect for Pattern B is the same: shifting the horizontal moisture-loaded wind circulation away from Southeast Amazon.

The *pull* factor determining the position and strength of Pattern B is the westerly Pacific Mid-Latitude Jet (MLJ). The MLJ is a key determinant on the pulling traction where

Relative humidity anom during HW10 and wind anom at 850 AMZ

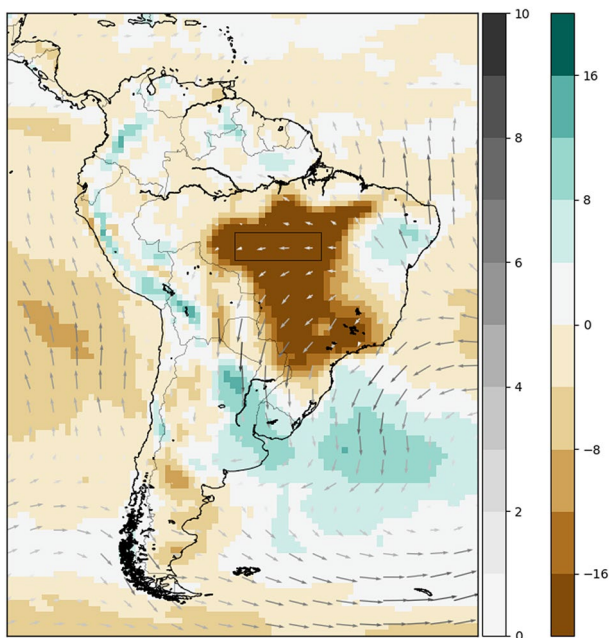


Fig. 5 Synoptic circulation anomalies at 850 hPa (vectors) and RH anomalies (shaded) during HW10. The grey scale reflects wind intensity (m/s) and brown-to-green RH anomalies (%)

the SALLJ flows to the South Atlantic. Wind field anomalies, in 8 out of 10 events (HW1, HW2, HW3, HW4, HW5, HW7, HW8, HW9 in Figs. S16, S17, S18, S19, S20, S22, S23, S24, respectively), show a strengthening (S16, S17, S18, S19, S20) or weakening (S22, S23, S24) of the South Pacific Low, which in either cases weaken the westerly flow of this jet passing through the southern tip of South America both at 850 and 200 hPa (figure not shown). Particularly, in HW1, HW2, HW3, HW4, HW5, this is diverting poleward this jet, away from the SALLJ usual trajectory and reducing the MLJ pull factor. In HW7, HW8 and HW9, the MLJ weakened due to a weaker Low. In HW6 (Fig. S21) and HW10 (Fig. 5, right panel) the jet is stronger as it flows further south towards the South Pole yet further away from the SALLJ usual trajectory. In all cases, the pull factor for Pattern B is reduced.

Altogether, the large-scale circulation anomalies during the 10 events shows a consistent (i) easterly advection of drier air into Southeast Amazon driven by the SAA. This additional dryness to an (ii) already dry surface (at the end of the dry season) is (iii) aggravated by a consistent diversion of moisture transport (in most cases to N → S) from Southeast Amazon. These three elements compounded together exacerbate dryness in the Southeast Amazon environment and are critical to escalate already hot temperatures to extreme heat.

5 Cross-section analysis of RH

Extreme dryness is found in mid to upper level in HW10 (Fig. 6) as well as in the remaining events (Figs. S24–S32). At surface, in all events the minimum RH is found to be persistently below 30%, particularly over the Eastern longitudes of the Eastern Amazon sub-region between 50° to 55°W. A strong and quick E–W gradient is visible in practically all events (except HW1) separating two markedly different vertical profiles of RH: a very humid surface drying with altitude (west of the gradient) and a very dry surface wetting with altitude (east of the gradient). This results in a surface gradient stretching from surface up to 800–700 hPa. Easterly surface advection seems to consistently have its maximum westward transport of drier air at 900 to 950 hPa up to around 57.5°W. In 5 out of 10 events (HW2, HW3, HW6, HW7, HW10 in Figs. S25, S26, S29, S30 and Fig. 6, respectively) a continuous dry air column (below 50% RH) stretches from surface to the upper troposphere (200 hPa). The 700 hPa layer is in all events the inversion point up to which RH increases from surface and from which it dries out up to 200 hPa. Therefore, it is the wettest level in the total column (with or without a dry column continuum). Altogether, the cross-section plots illustrate a consistent vertical structure with an intense dry signal at surface during all events.

In a comparison of the magnitude and vertical profile of RH, the heat wave and monthly climatological (Fig. 7) cross sections are compared.

The vertical profile of RH during most extreme heat-wave events (except HW1) presents similar features to the climatology which show three vertically distinguished components: a very dry layer at mid to top levels (600–300 hPa) and a humid layer at low to mid-levels (800–600 hPa) above the Southeast Amazon stretching east to the Atlantic Ocean. This layer engulfs a dry surface level (1000–800 hPa) ‘bubble’ located east of the 50°W meridian (where the Amazon frontier is).

However, a striking difference between the climatological and heat wave cross sections is found at the very surface layer (below 975 hPa) where a thin layer of 10–30% more humid air (in comparison to the surface of the ‘dry bubble’) stretches to the eastern ends of the Amazon frontier continuously from the wetter layers above the rainforest to the west. During all heat wave events however, this layer is absent indicating once more the significant influence of surface dryness in heat extremes in this region.

Another major difference found is that during all heat waves this thin layer of humid air was not only replaced by much drier air, but also was unusually drier and wider. In the climatological cross section, RH never goes below 40% in any segment of the section and never below 50%

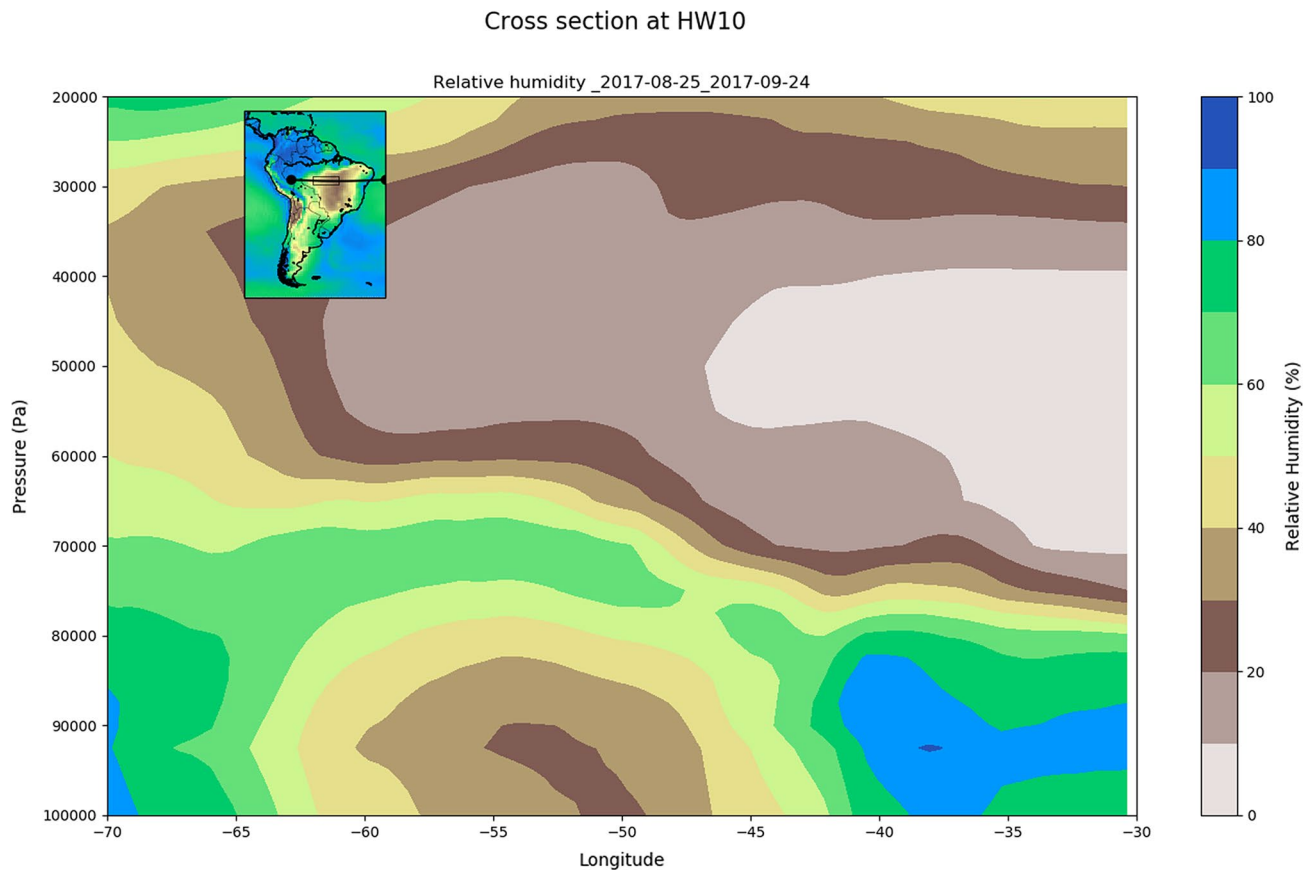


Fig. 6 Zonal cross section of RH during HW10 between 70°W and 30°W degrees at the central parallel of the Southeast Amazon subsection of 10°S. At the upper left corner, a map of South Amer-

ica shows the location of the cross section and the mean surface (1000 hPa) anomalies of RH during the event

over the Amazon forest. However, during almost all heat waves, this extreme dryness reaches low levels down to 20% and stretches westwards into the Amazon forest past the -60° W meridian. Noticeably as well, the contact of this dry bubble with the surface is widening in 9 out of 10 events exclusively westwards (it never expands eastwards), onto the Amazon forest.

The wind anomalies in Fig. 5 did not reveal a significant regional change over land in HW10, however in 7 out of 10 events (HW1, HW2, HW5, HW6, HW7, HW8, HW10), there was an increase in easterly advection within the Southeast Amazon region at this level. These results show that for most events, whilst the usual easterly circulation pattern in this season is maintained, it unusually stretched onto the Southeast frontier of the Amazon, contributing to an additional drying of an already dry surface.

An overall drier-than-normal state is visible across the entire domain in HW10 (see smaller sub-plot of RH mean anomalies at surface for the entire SA continent) in Fig. 8 (for the remaining events see figs S37 to S45). In 8 out of

10 cases, the driest anomalies are over the Southeast Amazon (see in the inset of figures S37, S38, S41, S42, S43, S44, S45 and Fig. 8). It is also consistently found in all events that at the land surface level, it is on the Southeast Amazon that the driest anomalies occur in the entire zonal cross-section. This adds to the previous analysis where, despite the vertical similarities between climatology and the events, the thin humidity layer found to be *missing* at surface during the events is significantly drier over Southeast than anywhere else at surface. The anomalies also indicate that the most substantial anomalous patterns are associated with an expansion westward of the driest surface air in the region. This dry surface air is usually confined to the NEB semi-arid and Cerrado regions, but during these events it extended onto the Amazon region.

Together with the results in Figs. 6, 7, 8, the heatwave events are found to relate to a westward extension of the dry conditions over the Cerrado and the semi-arid region in the NEB which are advected to the Amazon due to the surface level easterly wind anomalies.

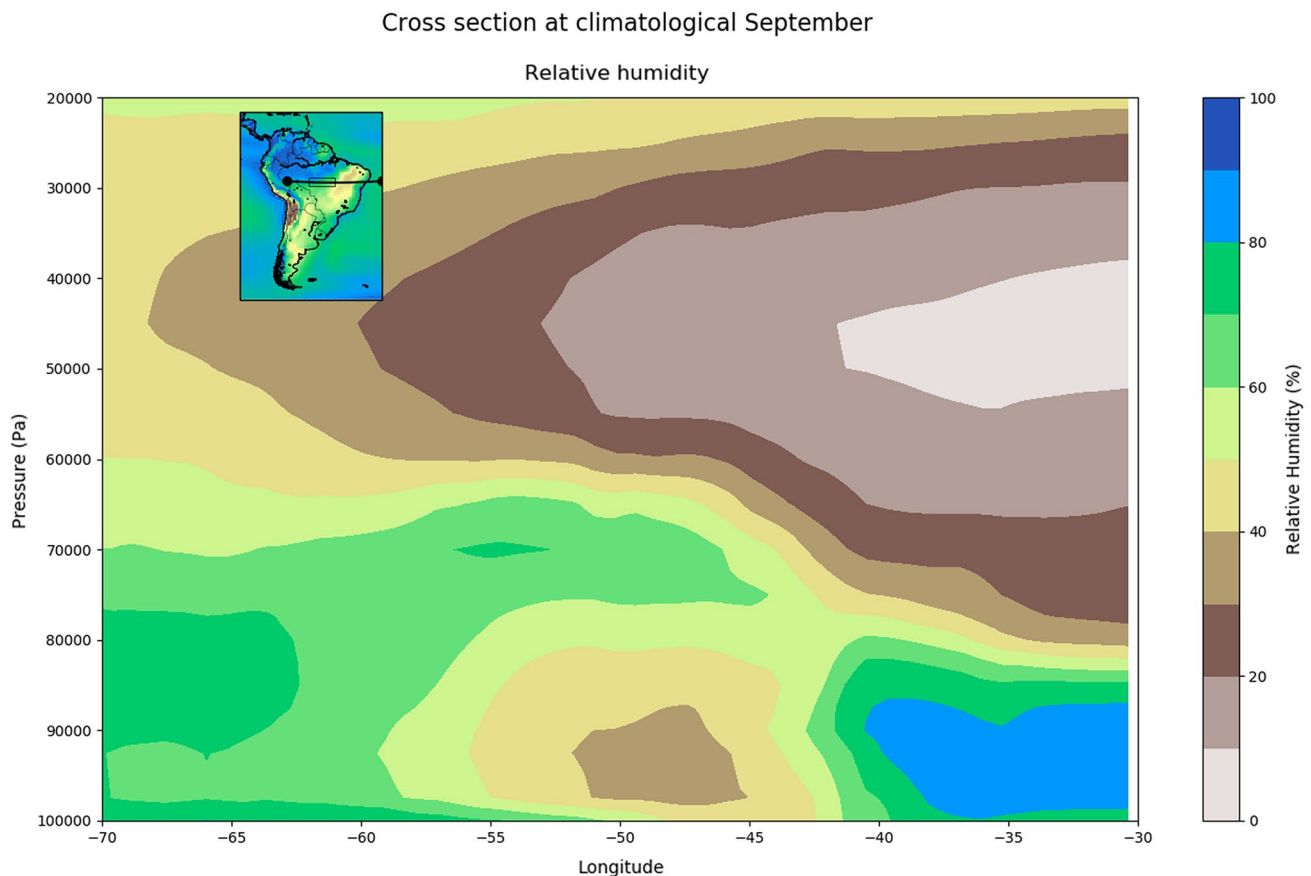


Fig. 7 As Fig. 6 but for the climatology of the month September (August, October and November are in Figs. S34, S35 and S36, respectively)

6 Exceptional heatwave events: HW1 and HW8—El Niño Southern Oscillation (ENSO) year events

In the case of HW8, which occurred in the El Niño year of 2015, the climatological cross sections revealed a vertical profile of RH (Fig. S32) typical of the dry season months of August (Fig. S34) or September (Fig. 7), yet happening in mid to late October. In ENSO years, the SAA anticyclonic circulation is intensified and with that the easterly advection through the NEB into the Amazon lasts into the SON season (Montini et al. 2019). This event is likely indicative of the consequences of the lengthening of the dry season which in the Amazon has already lengthened by 1 month since the 1970's (Marengo et al. 2018). It also illustrates the effects of changes in circulation during this season associated with El Niño, with consequences for extreme drought and heat (Fig. S23). El Niño has a significant effect on the SALLJ circulation with an increase in SALLJ days during the JJA and SON as a result of an intensification of the SAA easterly advection (Montini et al. 2019) instead of the SAMS. Unlike SAMS, this increase in SALLJ days driven by SAA leads to air with

lower moisture, expanding drier air to regions usually wetter such as the SE of Amazonia.

In the case of HW1, the large dry anomalies found in the cross-section (see Fig. S37) also helps to explain the exceptional case of this event. HW1 occurred in November, at the end of the SON season, and in 1997, right at the beginning of one of the strongest El Niño events on record (Huang et al. 2016). Therefore, this is a heat wave occurring outside of the dry season, which makes its circumstances different from all other events. Yet, like in the dry season, heat amplification in this case is also co-occurring together with anomalous drying.

The comparison between cross section profiles of Figs. S25 (absolute values of HW1) and S36 (climatology of November) shows drier RH conditions yet more humid than all other events. HW1 is an exceptional event as it does not relate with the climatological conditions of any of the months around its dates. The anomalies found here, however, provide the evidence that HW1 corresponded to very intense drying anomalies, vertically continuous, namely over the entire Amazon basin. Like in HW8, this is likely associated with the influence of a strong El Niño event in this region, yet the vertical profile of RH does not clearly show

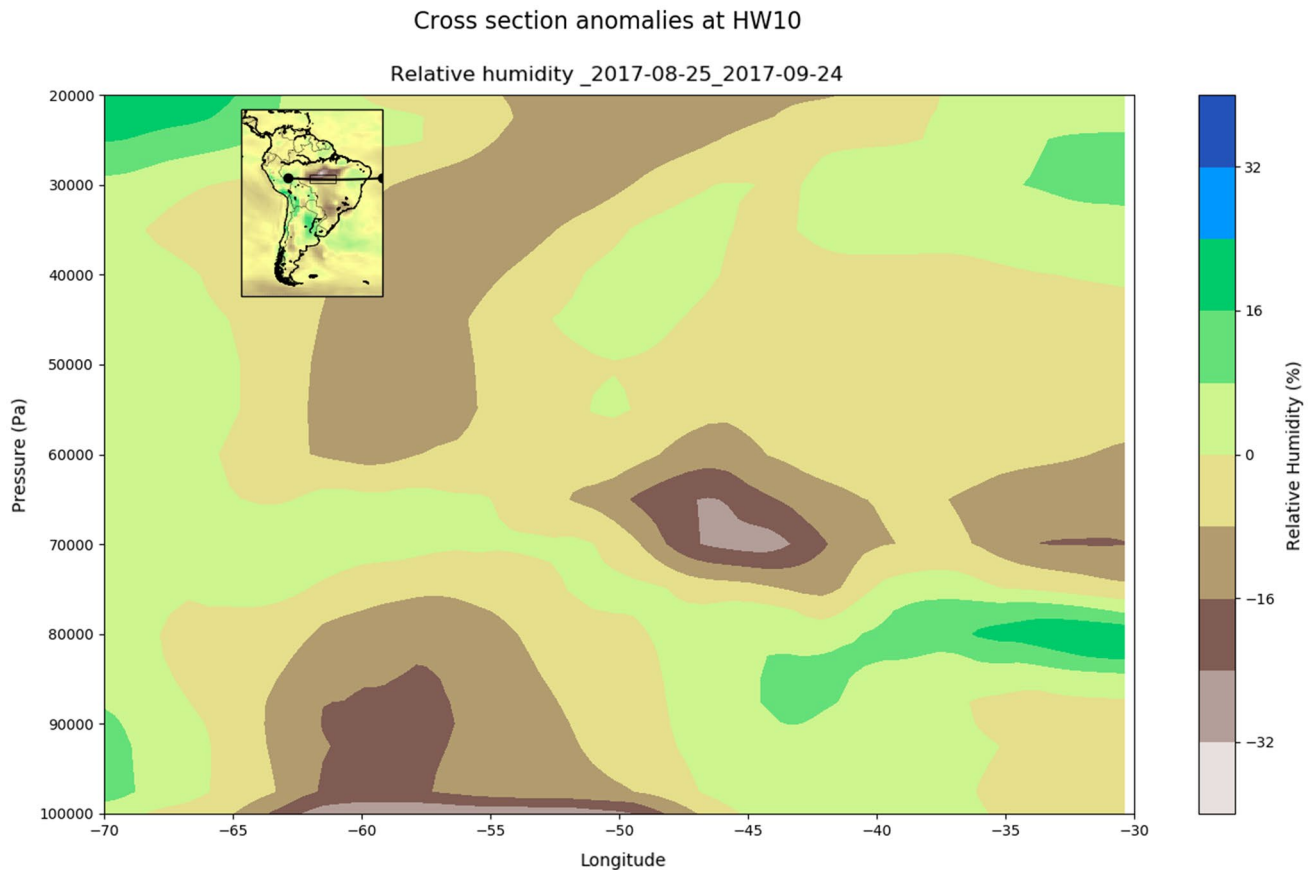


Fig. 8 As Fig. 6 but for RH anomalies

a structural pattern indicative of a lengthening of the dry season, such as in HW8.

7 Conclusions and discussion

This paper brings the first analysis of the atmospheric and surface conditions driving heat extreme events in the Amazon. From a sub-region in the eastern frontier of the Amazon, 10 of the longest and most intense events were identified and their drivers were analyzed. 9 out of 10 of these events occurred in the last decade. Our results indicate that these events may be triggered by anomalous large-scale atmospheric circulation and amplified by near-surface drying conditions.

Our analyses of synoptic wind patterns and anomalies showed consistently that during these events the seasonal easterly winds resulting from an intensified SAA and a weaker SAMS circulation advected onto the Amazon a much drier layer of air at surface. These easterly wind anomalies were particularly visible over the Southeast of the Amazon region in 7 out of 10 events (HW1, HW2, HW4, HW5, HW6, HW7, HW8, and HW 10). Dryness

is also associated with a shifted circulation of the SALLJ which reduced the influx of moisture into this region, further enhancing the drying conditions resulting from both the easterly advection and the already dry surface at the end of a prolonged dry season.

Our analysis of *push* and *pull* factors highlighted two wind circulation patterns in the event composites emerging from the intensification of the SAA that contribute to increased drying at surface: the easterly advection through the coast of the Northeast of Brazil into the Amazon (Pattern A) and the shift/suppression of the SALLJ flow pattern (Pattern B). These patterns depend on the position and strength of the synoptic conditions that both feed (*push factor*) and pull (*pull factor*) such air motion:

- In 10 out of 10 events where Pattern A is seen at 850 hPa in 9 of these strengthened by the intensification of the SAA
- In 10 out of 10 events, Pattern B reduces the influx of moisture into Southeast either due to its northerly positioning (during 9 out of 10 events) or being temporarily suppressed (during 1 out of 10 events).

It was found that in all events, heat extremes are coincident with extreme anomalous dryness both at the near-surface level of the atmosphere (RH) and at the land surface (EF). Anomalies of these during heat waves are also strongly and significantly correlated with tasmax anomalies. In theory, the amplification of heat from dryness happens as a result of a biophysical feedback from reduced evaporative cooling and enhanced sensible heating. EF was anomalously low which is consistent with this feedback. Yet, an intercomparison assessment of surface heat fluxes from the reanalysis products and flux tower data available in the Amazon is still necessary to confirm this association. The association between surface dryness and extreme heat is still made valid through the anomalously low levels of relative humidity. In all 10 events, RH and EF anomalies were on a strongly and statistically significant correlation with tasmax anomalies.

The cross-section analyses of RH visibly showed an intensification of surface drying during these events which consistently widened westwards from the Cerrado and semi-arid regions into the Amazon. In fact, comparing the vertical profiles of RH mean values during the heatwave events and the corresponding monthly climatology indicates clearly that it is near-surface levels, specifically over the Southeast of the Amazon, where the most significant drying occurs. Particularly, a thin wet surface layer above the rainforest to the west is anomalously absent during all heat waves. This is even clearer in the anomaly cross-sections which showed a general mesoscale dry anomaly during these events, where the near-surface layer over the Amazon was the most anomalously dry region in the entire zonal cross-section, even beyond the usually dry Cerrado and semi-arid regions.

Our results are consistent with the “dry an hot” conditions documented over other regions in literature (e.g., Senevirate et al. 2013; Donat et al. 2017; Vogel et al. 2017; McKinnon et al. 2021; Bryne 2021). For example, according to the theory based on atmospheric dynamics (Bryne 2021), warming is amplified for hot land days over tropical land because those days are dry, which is termed the ‘drier get hotter’ mechanism. Changes in near-surface RH further increase tropical land warming, with decreases in land RH being particularly important. The theory highlights land surface dryness as a key factor determining how extreme temperatures respond to climate change over tropical land, particularly during the warm season in moist regions such as the Amazon rainforest where warming is largely amplified when ET is supposed (e.g., Duan et al. 2020; Ionita et al. 2021).

There are some important limitations and caveats to mention in this study, which may hopefully be addressed in future research:

Deforestation – Southeastern Amazon is a highly deforested section of the Amazon, at the centre of the Arc of Deforestation. In the ERAI assimilations how-

ever, there is no deforestation, i.e. vegetation cover and type are an invariant field in the reanalysis model with almost 100% cover of evergreen broadleaf trees. However, since the reanalysis model assimilates observational satellite data from both the atmosphere (like temperature and humidity) and the land surface (such as soil moisture) over this region, it may be biased from *assimilating* to a forest context (in the model) land-atmosphere observations of a mostly degraded and deforested grassland environment.

SALLJ – The classification of *SALLJ days* depends on the type of criteria chosen for its identification, which depends on the wind conditions at 850 hPa in two specific locations outside of this region (Montini et al. 2019; Marengo et al. 2011; Silva 2010; Bonner 1968). To therefore associate the amplification of heat extremes with the SALLJ moisture transport, it would be required to apply one set of criteria and compare the wind and heat conditions in SALLJ and non-SALLJ days. In this paper, the wind analysis considers wind patterns consistent with the SALLJ seasonal patterns and associates these with the advection of dryness (in the case of process A) and lack of humidity transport (in process B). Analysing on a daily scale the effects of SALLJ flow versus SALLJ suppression during heat waves will advance our understanding of the role of this mechanism during heat waves. That, however, was outside of the scope of this analysis.

El Niño – Two of the heatwaves analysed here (HW1 and HW8) occurred in two of the strongest El Niño years of 1997 and 2015. These were also the only two events of extreme heat occurring between August and September, outside of the hottest season of the year in the Southeast Amazon. These two events were consistent with all the other events in the levels of anomalous heat and surface dryness, a feature that is a key part of the atmospheric conditions leading to a heat wave event. These events may serve as a case study of heat extremes occurring during El Niño events, in one case associated with a lengthening of the dry season (HW8) and, in another, with an extreme dry anomaly at the onset of the wet season (HW1).

In conclusion, this study is a first reanalysis evidence of both the occurrence of heat extremes in Amazonia and their land and atmospheric drivers. It delivers unequivocal finding of the co-occurrence of extreme surface dryness with extreme heatwaves and lays the foundation for a more process-based analysis of the land-surface biophysical feedback from extreme dryness on surface temperatures in the context of a tropical rainforest under great anthropic pressure like the Amazon.

Supplementary Information The online version contains supplementary material available at <https://doi.org/10.1007/s00382-021-06134-8>.

Acknowledgements Helber B. Gomes acknowledges the Conselho Nacional de Desenvolvimento Científico e Tecnológico (CNPq) support through Grant no. 405664/2018-4.

References

- Almeida CT et al (2017a) Spatiotemporal rainfall and temperature trends throughout the Brazilian Legal Amazon, 1973–2013. *Int J Climatol* 37(4):2013–2026
- Almeida VA, Marton E, Nunes AMB (2017b) Assessing the ability of three global reanalysis products to reproduce South American monsoon precipitation. *Atmosfera* 31(1):1–10
- Alves LM et al (2017) Sensitivity of Amazon Regional climate to deforestation. *Am J Clim Chang* 06(01):75–98
- Bannister RN (2001) Elementary 4d-var. Reading: University of Reading. Available at: <http://www.met.rdg.ac.uk/~ross/Documents/Var4d.pdf>
- Bitencourt DP et al (2016) Frequência, Duração, Abrangência Espacial e Intensidade das Ondas de Calor no Brasil. *Revista Brasileira De Meteorologia* 31(4):506–517
- Bonner WD (1968) Climatology of the low level jet. *Mon Weather Rev* 96(12):833–850
- Brouillet A, Joussaume S (2019) Investigating the role of the relative humidity in the co-occurrence of temperature and heat stress extremes in CMIP5 projections. *Geophys Res Lett* 46(11):435–443
- Byrne MP (2021) Amplified warming of extreme temperatures over tropical land. *Nat Geosci* 14:837–841
- De Barros SD, Lee H, Loikith PC (2017) Can significant trends be detected in surface air temperature and precipitation over South America in recent decades? *Int J Climatol*. <https://doi.org/10.1002/joc.4792>
- Decker M et al (2012) Evaluation of the reanalysis products from GSFC, NCEP, and ECMWF using flux tower observations. *J Clim* 25(6):1916–1944
- Dee DP et al (2011) The ERA-Interim reanalysis: configuration and performance of the data assimilation system. *Q J R Meteorol Soc* 137:553–597
- Donat MG, Pitman AJ, Seneviratne SI (2017) Regional warming of hot extremes accelerated by surface energy fluxes: accelerated warming of hot extremes. *Geophys Res Lett* 44(13):7011–7019
- Duan SQ, Findell KL, Wright JS (2020) Three regimes of temperature distribution change over dry land, moist land, and oceanic surfaces. <https://doi.org/10.1029/2020GL090997>
- Espinoza JC et al (2018) Contrasting North-South changes in Amazon wet-day and dry-day frequency and related atmospheric features (1981–2017). *Clim Dyn*. <https://doi.org/10.1007/s00382-018-4462-2>
- Fischer EM et al (2007) Soil Moisture-Atmosphere Interactions during the 2003 European Summer Heat Wave. *J Clim* 20(20):5081–5099
- Flores BM et al (2017) Floodplains as an Achilles' heel of Amazonian forest resilience. *Proc Natl Acad Sci USA* 114(17):4442–4446
- Geirinhas JL et al (2018) Climatic and synoptic characterization of heat waves in Brazil. *Int J Climatol* 38(4):1760–1776
- Gloor M et al (2015) Recent Amazon climate as background for possible ongoing and future changes of Amazon humid forests: AMAZON CLIMATE AND TROPICAL FORESTS. *Global Biogeochem Cycles* 29(9):1384–1399
- Gomes HB et al (2019) Climatology of easterly wave disturbances over the tropical South Atlantic. *Clim Dyn*. <https://doi.org/10.1007/s00382-019-04667-7>
- Hartmann DL et al. (2013) Observations: atmosphere and surface. In *Climate Change 2013 the Physical Science Basis: Working Group I Contribution to the Fifth Assessment Report of the Intergovernmental Panel on Climate Change*. Cambridge University Press
- Hirsch AL et al (2015) Modulation of land-use change impacts on temperature extremes via land-atmosphere coupling over Australia. *Earth Interact* 19(12):1–24
- Huang B et al (2016) Ranking the strongest ENSO events while incorporating SST uncertainty. *Geophys Res Lett* 43(17):9165–9172
- Ionita M et al (2021) Compound hot and dry events in Europe: variability and large-scale. Drivers. <https://doi.org/10.3389/fclim.2021.688991>
- Jiménez-Muñoz JC et al (2013) Spatial and temporal patterns of the recent warming of the Amazon forest. *J Geophys Res Atmos* 118(11):5204–5215
- Jiménez-Muñoz JC et al (2016) Record-breaking warming and extreme drought in the Amazon rainforest during the course of El Niño 2015–2016. *Sci Rep* 6:33130
- Liebmann B, Mechoso CR (2011) The South American Monsoon System. In *The Global Monsoon System*. World Scientific Series on Asia-Pacific Weather and Climate. WORLD SCIENTIFIC 137–157.
- Lorenz C, Kunstmann H (2012) The hydrological cycle in three state-of-the-art reanalyses: intercomparison and performance analysis. *J Hydrometeorol* 13(5):1397–1420
- Marengo JA et al (2004) Climatology of the low-level jet east of the andes as derived from the NCEP–NCAR reanalyses: characteristics and temporal variability. *J Clim* 17(12):2261–2280
- Marengo JA et al (2011) The drought of 2010 in the context of historical droughts in the Amazon region. *Geophys Res Lett*. <https://doi.org/10.1029/2011GL047436>
- Marengo JA et al (2018) Changes in climate and land use over the amazon region: current and future variability and trends. *Front Earth Sci China* 6:228
- McKinnon KA, Poppick A, Simpson IR (2021) Hot extremes have become drier in the United States Southwest. *Nat Clim Chang* 11:598–604
- Miralles DG et al (2014) Mega-heatwave temperatures due to combined soil desiccation and atmospheric heat accumulation. *Nat Geosci* 7:345
- Montini TL, Jones C, Carvalho LMV (2019) The South American low-level jet: a new climatology, variability, and changes. *J Geophys Res Atmos* 124(3):1200–1218
- Observatory NE (2010) World of Change: Global Temperatures. Available at: <https://earthobservatory.nasa.gov/WorldOfChange/DecadalTemp>. Accessed October 11, 2018
- Perkins SE (2015) A review on the scientific understanding of heatwaves—Their measurement, driving mechanisms, and changes at the global scale. *Atmos Res* 164–165:242–267
- Seneviratne SI et al (2013) Impact of soil moisture-climate feedbacks on CMIP5 projections: first results from the GLACE-CMIP5 experiment. *Geophys Res Lett* 40:5212–5217
- Silva GAM, Ambrizzi T, Marengo JA (2009) Observational evidences on the modulation of the South American low level Jet east of the Andes according to the ENSO variability. *Ann Geophys* 27:645–657
- Silva MCL, da Rocha RP, Ynoue RY (2010) Climatic simulations of the eastern Andes low-level jet and its dependency on convective parametrizations. *Meteorol Atmos Phys*. <https://doi.org/10.1007/s00703-010-0077-9>
- Skansi MLM et al (2013) Warming and wetting signals emerging from analysis of changes in climate extreme indices over South America. *Global Planet Change* 100:295–307

- Ukkola AM et al (2018) Evaluating the contribution of land-atmosphere coupling to heat extremes in CMIP5 models. *Geophys Res Lett* 45(17):9003–9012
- Vogel MM et al (2017) Regional amplification of projected changes in extreme temperatures strongly controlled by soil moisture–temperature feedbacks. *Geophys Res Lett* 44:1511–1519

Publisher's Note Springer Nature remains neutral with regard to jurisdictional claims in published maps and institutional affiliations.